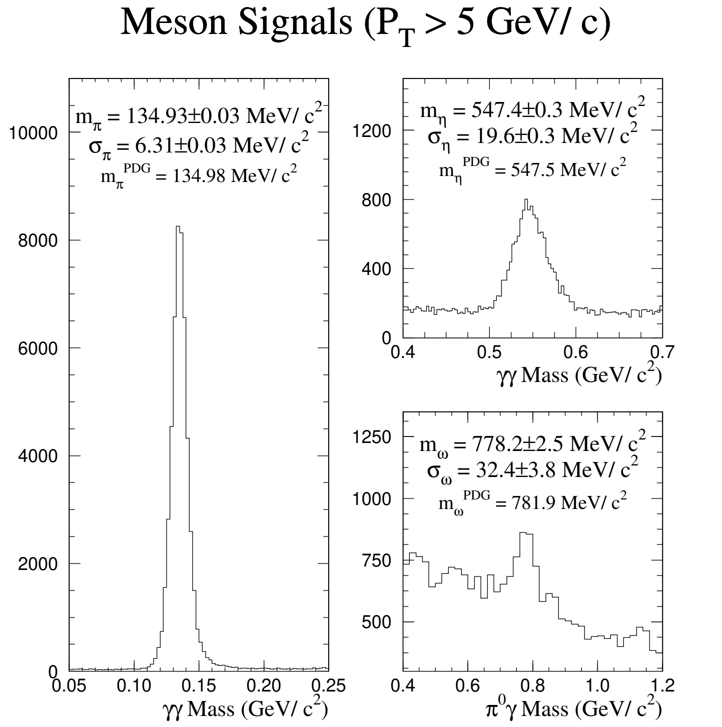

Figure 1: The reconstructed masses of high-p_T π^0, η, and ω mesons in all-photon final states.

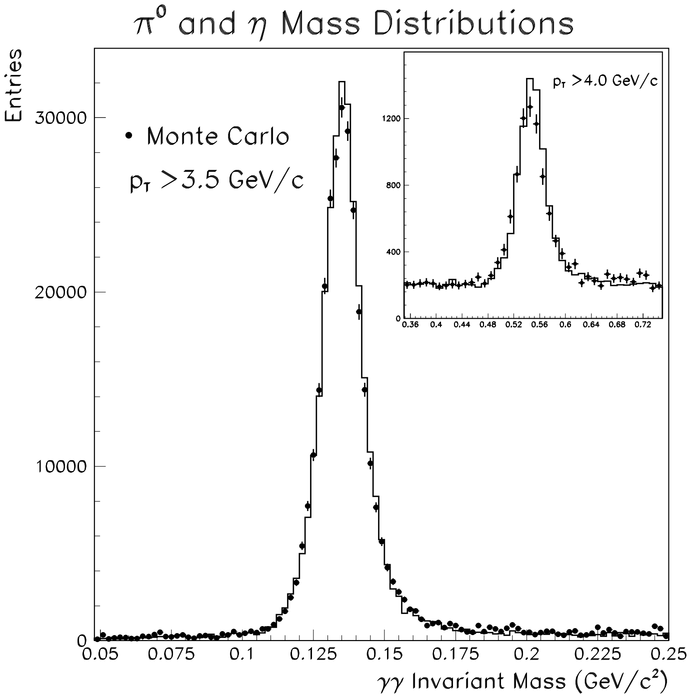

Figure 3: A comparison of the two-photon mass distributions from the incident π^- beam data and from the corresponding Monte Carlo simulation. The distributions exhibit prominent π^0 and η peaks.

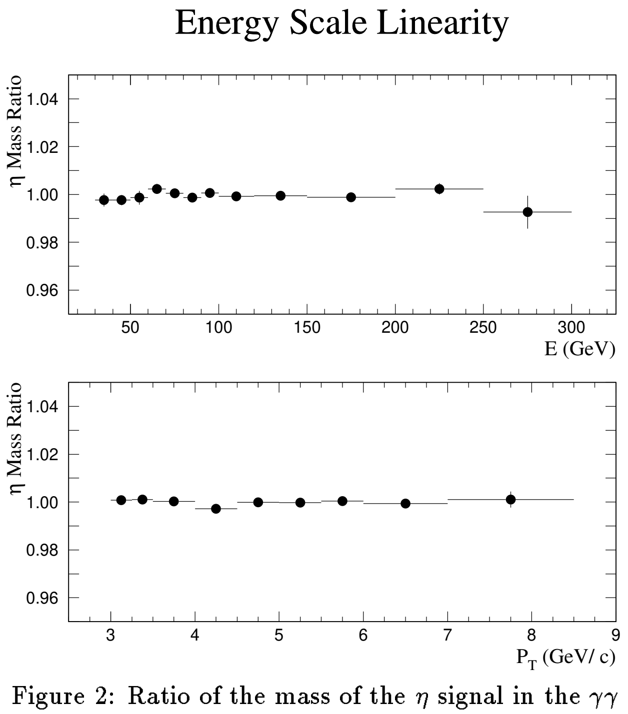

Figure 2: Ratio of the mass of the η signal in the $\gamma\gamma$ decay mode to its nominal value as a function of the energy (top plot) and p_T (bottom plot) of the $\gamma\gamma$ pair.

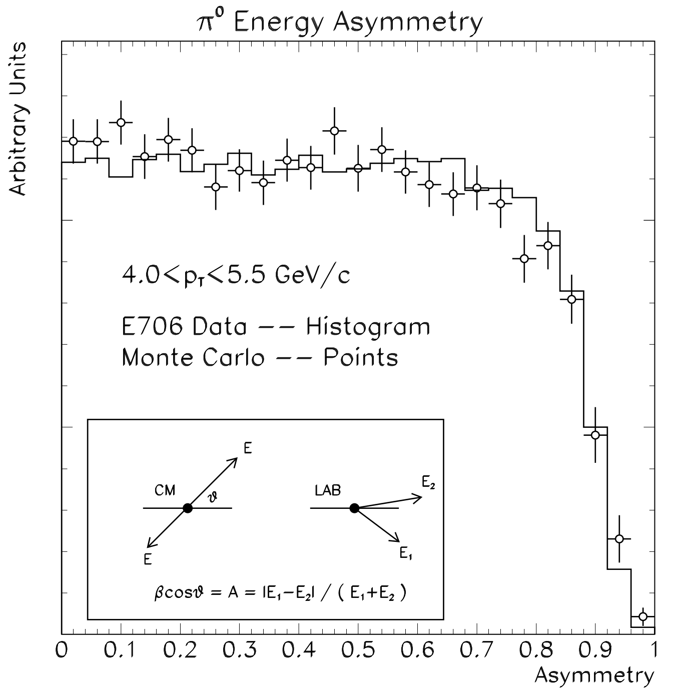

Figure 4: A comparison of the background-subtracted energy asymmetry distribution for photons from π^0 decays from the incident π^- beam data and from the corresponding Monte Carlo simulation. The π^0's have p_T's between 4.0 GeV/c and 5.5 GeV/c.

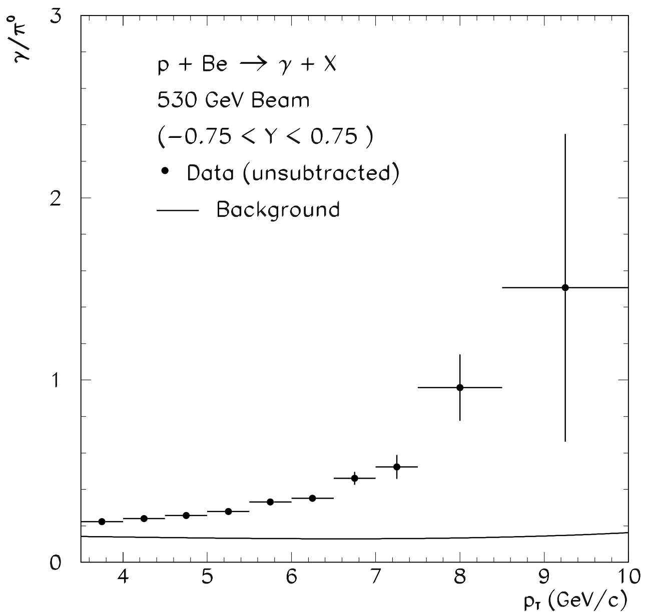

Figure 5: The ratio of the single photon cross section to the π^0 cross section as a function p_T from interactions of 530 GeV/c protons incident on beryllium. The curve shows the contribution to the single photon cross section due to sources other than direct photon production as determined via a detailed Monte Carlo simulation.

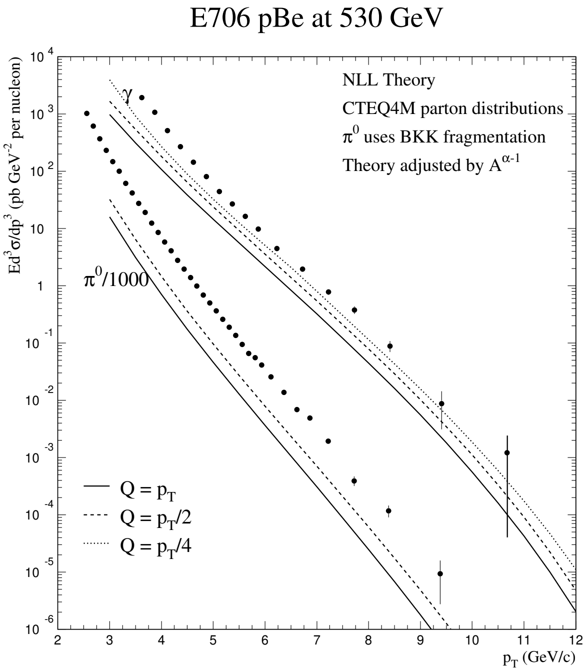

Figure 6: The π^0 and direct photon inclusive cross sections as a function of p_T for 530 GeV/c proton-nucleon interactions. The data are compared to NLL pQCD calculations for several choices of the renormalization and factorization scales (the pQCD calculation of the π^0 cross section using $Q = p_T/4$ breaks down for $p_T < 6$ GeV/c). The π^0 cross section has been multiplied by a factor of 0.001 for display purposes.

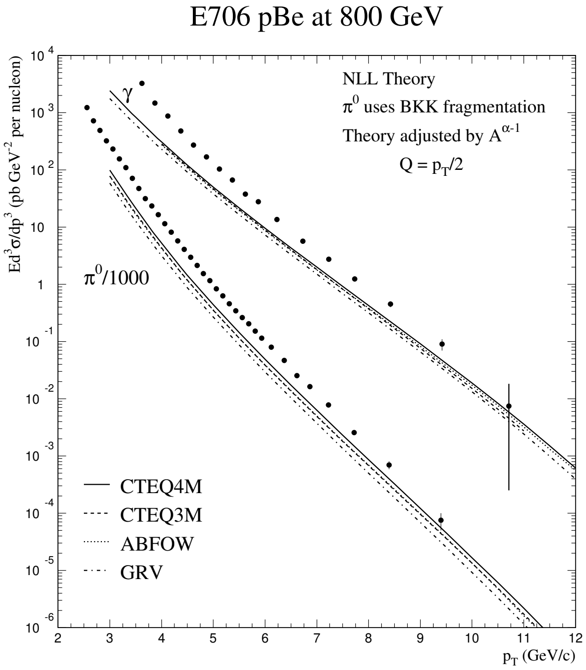

Figure 7: The π^0 and direct photon inclusive cross sections as a function of p_T for 800 GeV/c proton-nucleon interactions. The data are compared to the results of NLL pQCD calculations for several choices of the parton distribution functions. The π^0 cross section has been multiplied by a factor of 0.001 for display purposes.

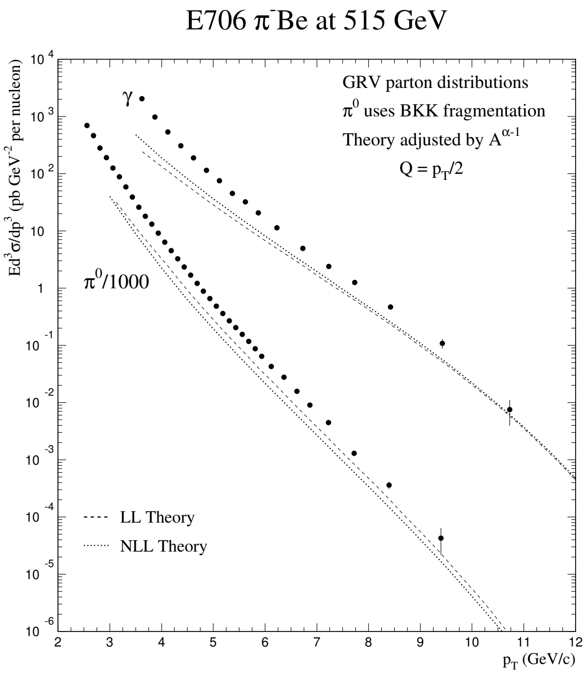

Figure 8: The π^0 and direct photon inclusive cross sections as a function of p_T for 515 GeV/c π^--nucleon interactions. The data are compared to results of LL and NLL pQCD calculations. The π^0 cross section has been multiplied by a factor of 0.001 for display purposes.

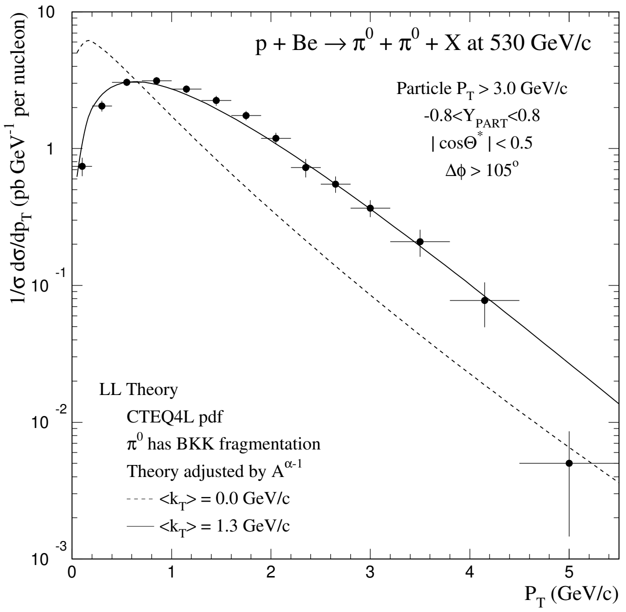

Figure 9: The distribution of the p_T of pairs of high-p_T π^0's produced in interactions of 530 GeV/c protons incident on a beryllium target. The dashed curve shows the results of a LL calculation of the corresponding distribution when the incident partons have an $\langle k_T \rangle$ of 0, while the solid curve shows the corresponding result when $\langle k_T \rangle = 1.3$ GeV/c.

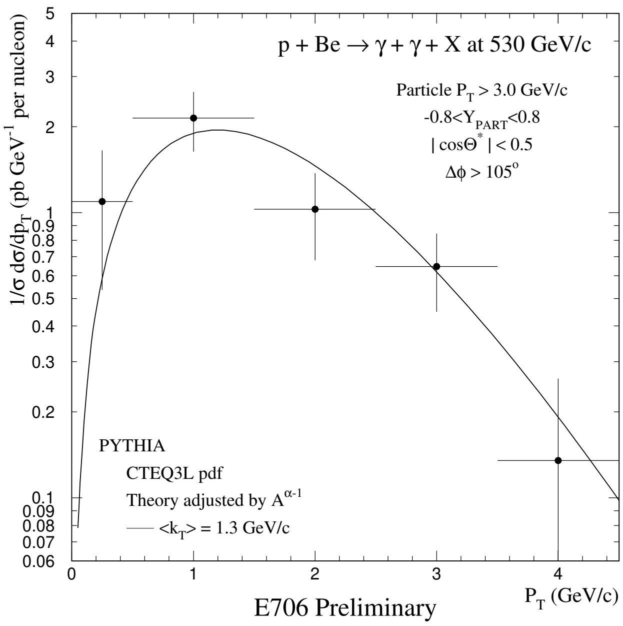

Figure 11: The distribution of the p_T of pairs of direct photons produced in interactions of incident 530 GeV/c protons on beryllium. The solid curve shows the results of a PYTHIA calculation of the pair p_T distribution for $\langle k_T \rangle = 1.3$ GeV/c. At leading order, the corresponding curve for $k_T = 0$ is a delta function at $p_T = 0$.

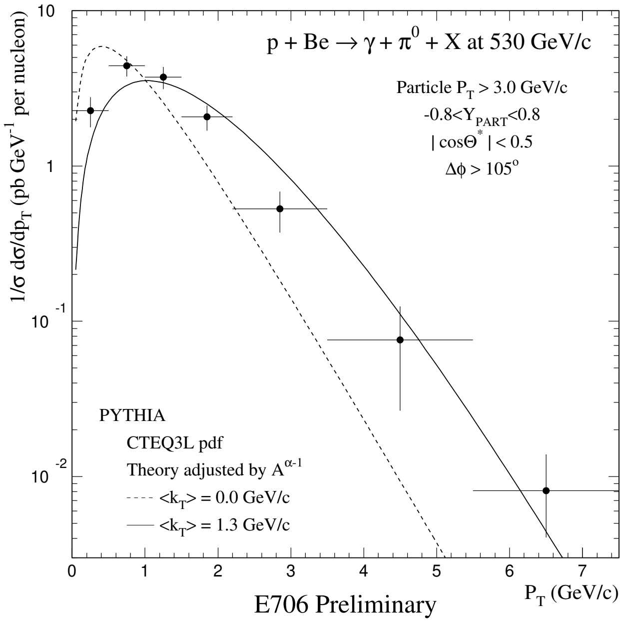

Figure 10: The distribution of the p_T of direct photon-π^0 pairs produced in interactions of incident 530 GeV/c protons on beryllium. The dashed curve shows the results of a PYTHIA calculation of the pair p_T distribution for $\langle k_T \rangle = 0$, while the solid curve shows the corresponding result for $\langle k_T \rangle = 1.3$ GeV/c.

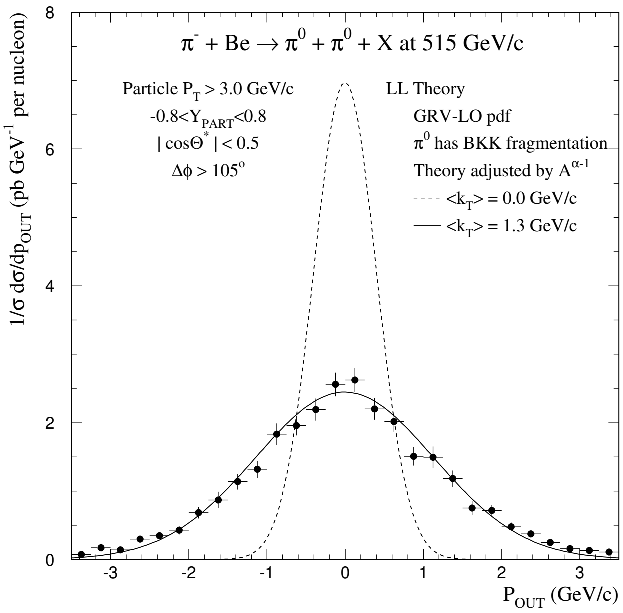

Figure 12: The out-of-plane momentum distribution from pairs of high-p_T π^0's produced in π^--nucleon interactions at 515 GeV/c compared to results from LL calculations for two values of $\langle k_T \rangle$.

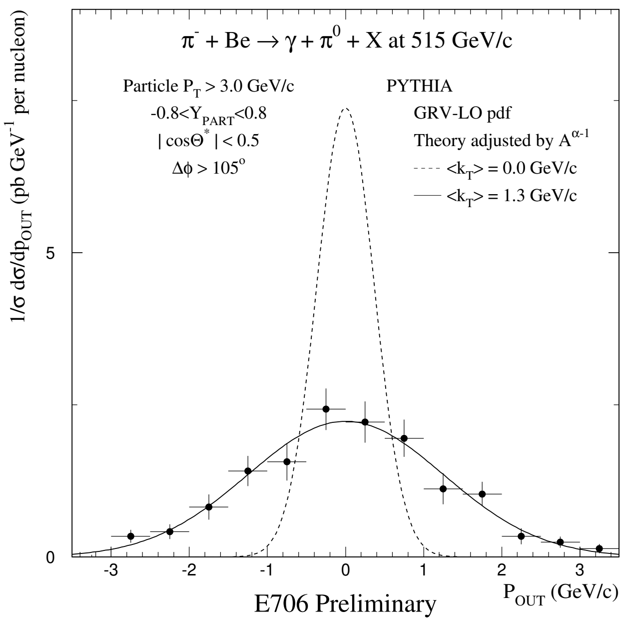

Figure 13: The out-of-plane momentum distribution for γ π^0 pairs produced in π^--nucleon interactions at 515 GeV/c compared to results from PYTHIA for two values of $\langle k_T \rangle$.

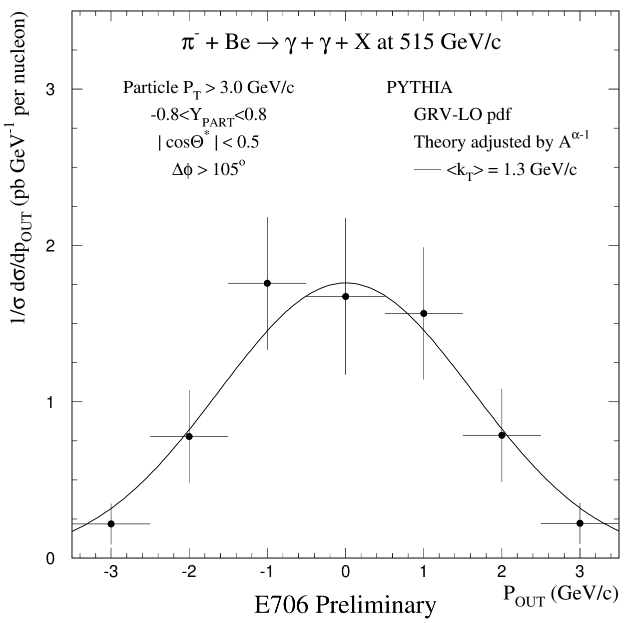

Figure 14: The out-of-plane momentum distribution for pairs of direct photons produced in π^--nucleon interactions at 515 GeV/c compared to results from PYTHIA with $\langle k_T \rangle$ = 1.3 GeV/c. At leading order, the corresponding $k_T = 0$ curve is a delta function at $p_{\rm out} = 0$.

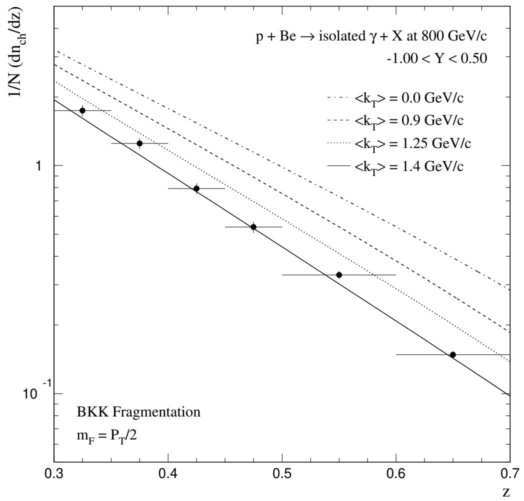

Figure 15: The fragmentation distribution for charged particles recoiling against isolated photons with p_T > 5.5 GeV/c produced in 800 GeV/c proton-nucleon interactions. z is the component of the momentum of the individual charged particle relative to the recoil jet momentum, where the recoil jet transverse momentum has been rescaled to match the isolated photon's transverse momentum. The distribution is compared to expectations based upon calculations using BKK fragmentation supplemented with several choices of $\langle k_T \rangle$.

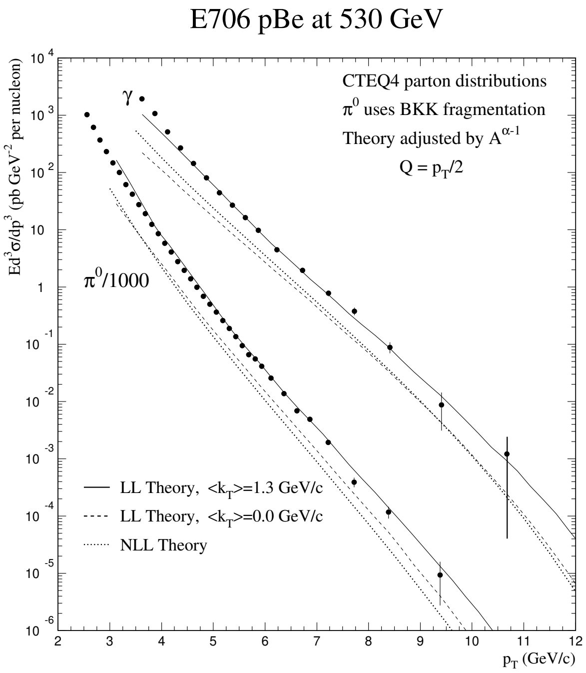

Figure 16: The π^0 and direct photon inclusive cross sections as a function of p_T for 530 GeV/c proton-nucleon interactions. The data are compared to the results of a LL pQCD calculation, a LL pQCD calculation supplemented with an $\langle k_T \rangle$ of 1.3 GeV/c, and a NLL pQCD calculation. The π^0 cross section has been multiplied by a factor of 0.001 for display purposes.

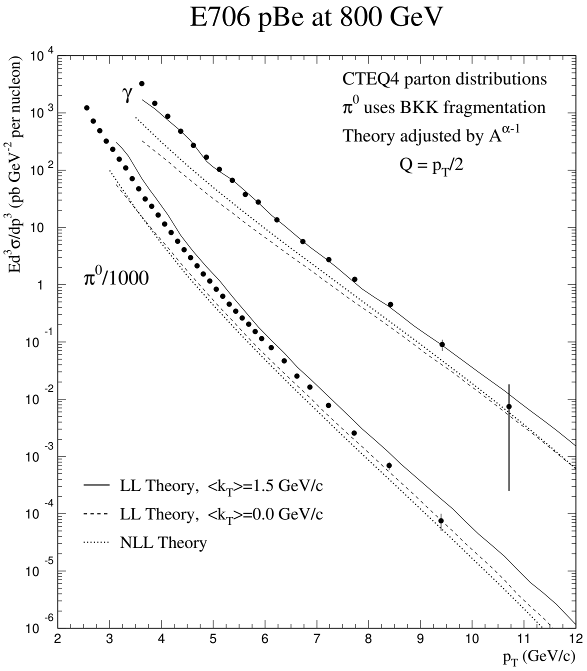

Figure 17: The π^0 and direct photon inclusive cross sections as a function of p_T for 800 GeV/c proton-nucleon interactions. The data are compared to the results of a LL pQCD calculation, a LL pQCD calculation supplemented with an $\langle k_T \rangle$ of 1.5 GeV/c, and a NLL pQCD calculation. The π^0 cross section has been multiplied by a factor of 0.001 for display purposes.

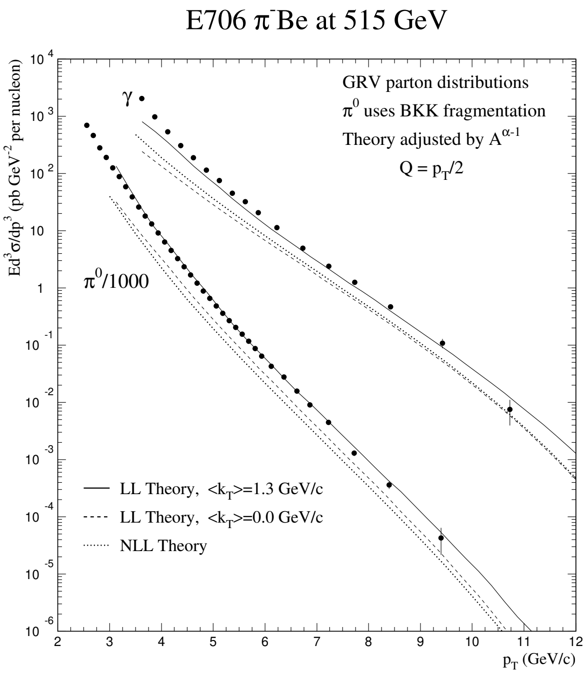

Figure 18: The π^0 and direct photon inclusive cross sections as a function of p_T for 515 GeV/c π^--nucleon interactions. The data are compared to the results of a LL pQCD calculation, a LL pQCD calculation supplemented with an $\langle k_T \rangle$ of 1.3 GeV/c, and a NLL pQCD calculation. The π^0 cross section has been multiplied by a factor of 0.001 for display purposes.

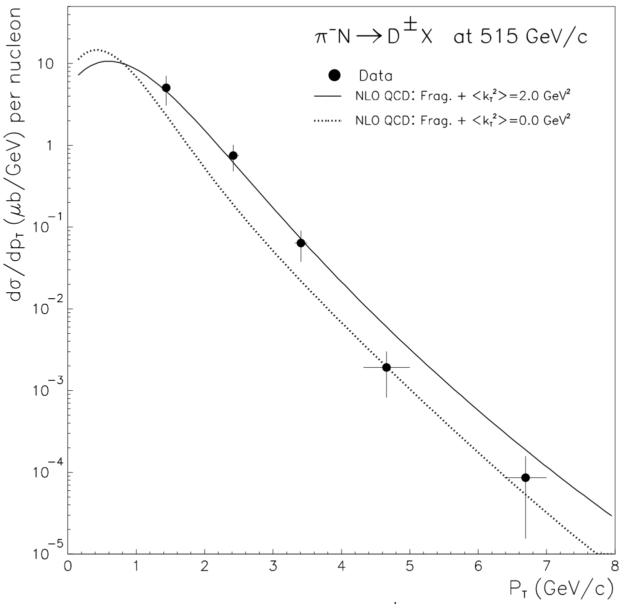

Figure 19: Comparison of the $D^{\pm}$ differential cross section per nucleon measured by experiment E706 to results of NLO pQCD calculations supplemented with average transverse momenta squared ($\langle k_T^2 \rangle$) of 0, or 2.0 (GeV/c)^2. The charm quark mass employed in these calculations was 1.5 GeV/c^2. The NLO pQCD cross sections are normalized to our extrapolated integrated charged D cross section. Error bars represent statistical and systematic uncertainties added in quadrature, excluding luminosity and branching ratio contributions.

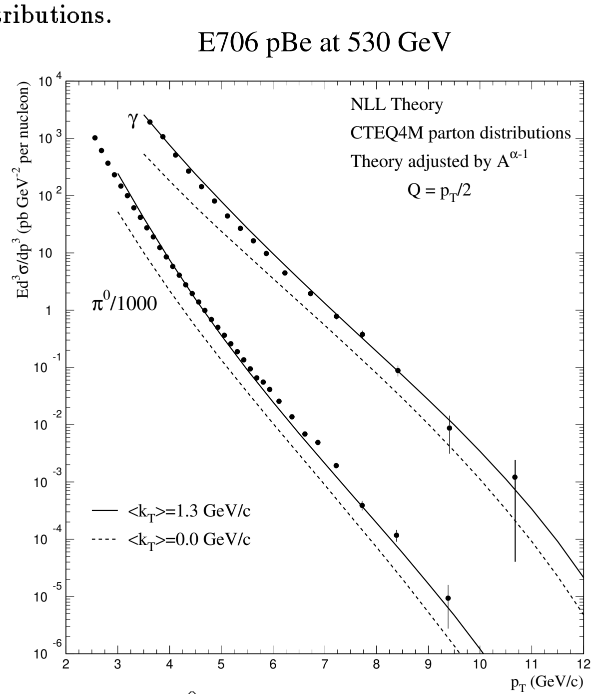

Figure 20: The π^0 and direct photon inclusive cross sections as a function of p_T for 530 GeV/c proton-nucleon interactions. The data are compared to the results of NLL pQCD calculations without supplemental k_T and with an $\langle k_T \rangle$ of 1.3 GeV/c. The displayed π^0 cross section has been multiplied by a factor of 0.001 for display purposes.

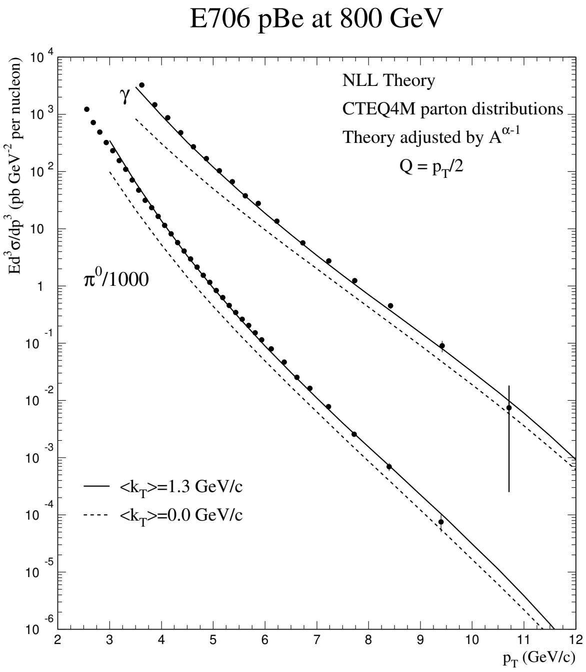

Figure 21: The π^0 and direct photon inclusive cross sections as a function of p_T for 800 GeV/c proton-nucleon interactions. The data are compared to the results of NLL pQCD calculations without supplemental k_T and with an $\langle k_T \rangle$ of 1.3 GeV/c. The displayed π^0 cross section has been multiplied by a factor of 0.001 for display purposes.

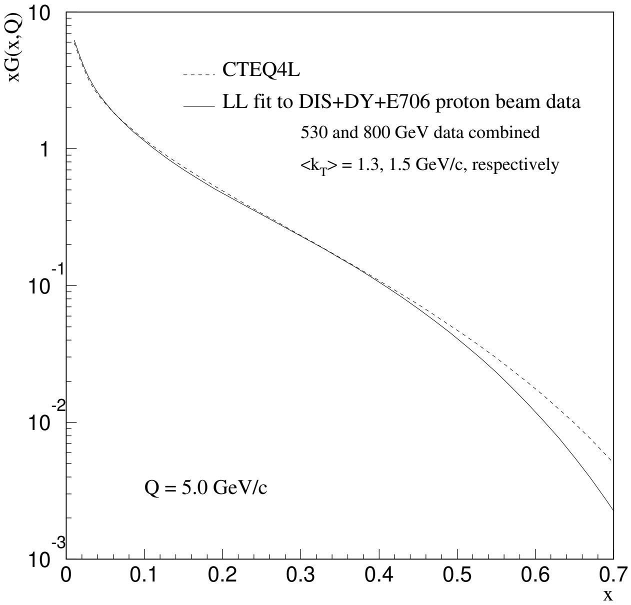

Figure 23: xG(x) of the nucleon as a function of x at $Q = 5$ GeV/c for the gluon determined by a LL fit to data from DIS, Drell-Yan, and the E706 direct photon cross sections. The plot also shows the corresponding distribution of xG(x) for the gluon from the CTEQ4L parton distribution functions.

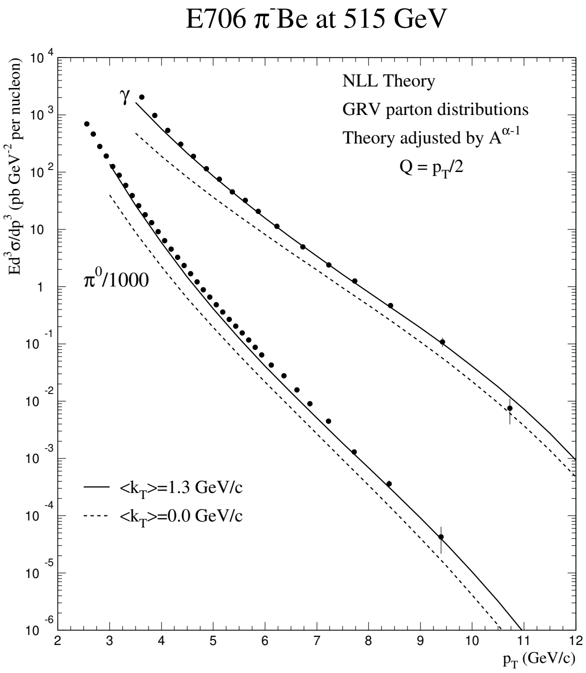

Figure 22: The π^0 and direct photon inclusive cross sections as a function of p_T for 515 GeV/c π^--nucleon interactions. The data are compared to the results of NLL pQCD calculations without supplemental k_T and with an $\langle k_T \rangle$ of 1.3 GeV/c. The displayed π^0 cross section has been multiplied by a factor of 0.001 for display purposes.

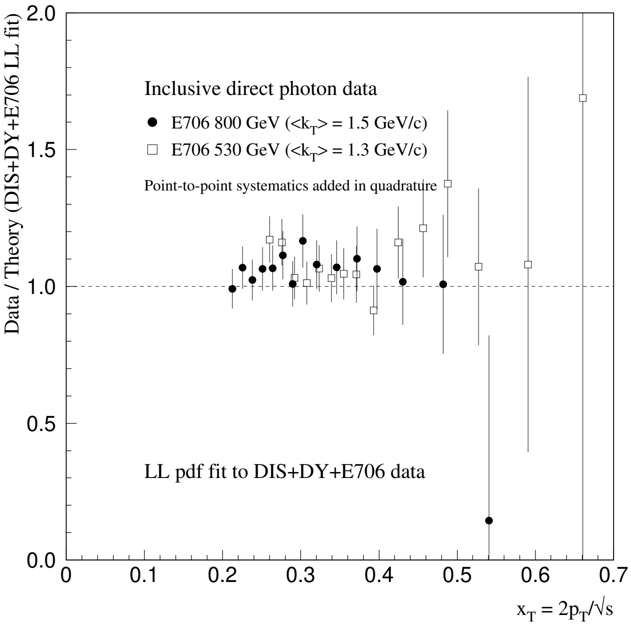

Figure 24: Ratio of our measured direct photon cross sections as a function of $x_T \equiv 2p_T/\sqrt{s}$ for incident 530 and 800 GeV/c proton beams to the cross section resulting from a LL calculation using the gluon determined by fitting data from DIS, Drell-Yan, and the E706 direct photon cross sections.

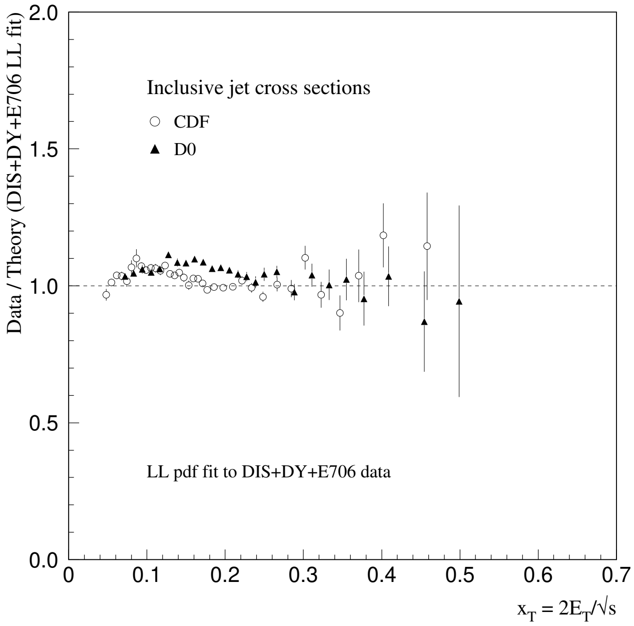

Figure 25: Ratio of high transverse energy jet cross sections as a function of the scaled E_T $(2E_T/\sqrt{s})$ measured by D0 and CDF to the corresponding cross section resulting from a LL calculation using the gluon determined by fitting data from DIS, Drell-Yan, and the E706 direct photon cross sections.

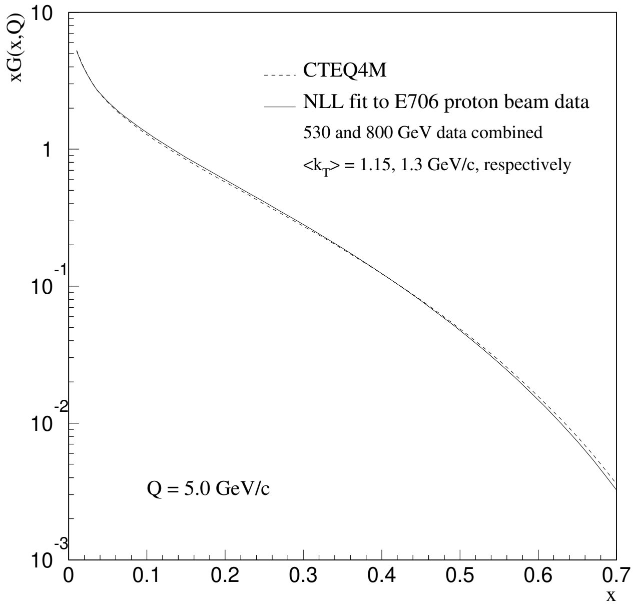

Figure 26: xG(x) of the nucleon as a function of x at $Q = 5$ GeV$/c$ for the gluon determined by a NLL fit to data from DIS, Drell-Yan, and the E706 direct photon cross sections. The plot also shows the corresponding distribution of xG(x) for the gluon from the CTEQ4M parton distribution functions.

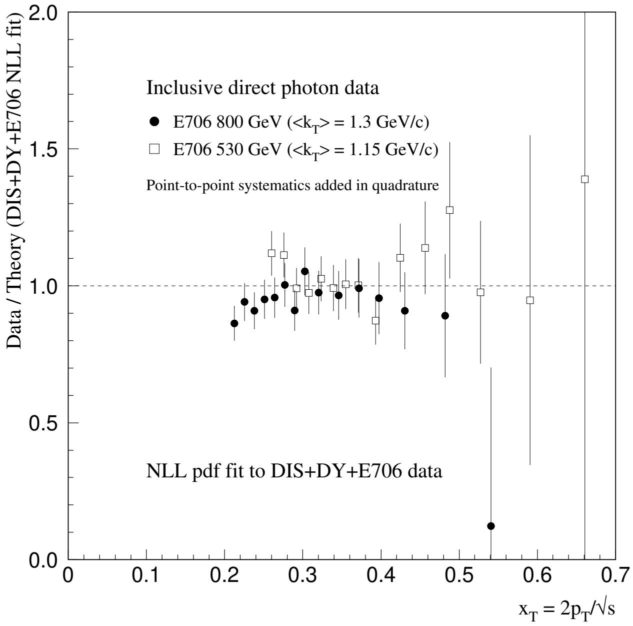

Figure 27: Ratio of our measured direct photon cross sections as a function of $x_T \equiv 2p_T/\sqrt{s}$ for incident 530 and 800 GeV$/c$ proton beams to the cross section resulting from a NLL calculation using the gluon determined by fitting data from DIS, Drell-Yan, and the E706 direct photon cross sections.

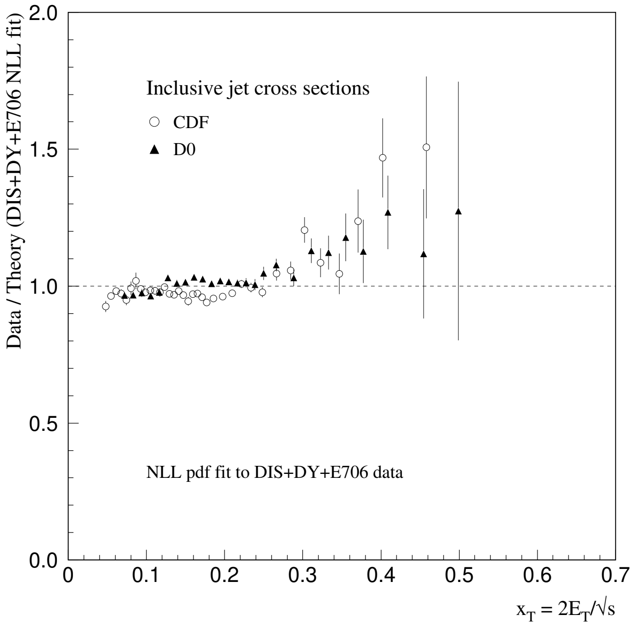

Figure 28: Ratio of high transverse energy jet cross sections as a function of the scaled E_T $(2E_T/\sqrt{s})$ measured by CDF and D0 to the corresponding cross section resulting from a NLL calculation using the gluon determined by fitting data from DIS, Drell-Yan, and the E706 direct photon cross sections.